nature communications

Article

https://doi.org/10.1038/s41467-026-70096-w

Rumor propagation on hypergraphs

Received: 5 September 2025

Accepted: 17 February 2026

Published online: 26 February 2026

Check for updates

Kleber Andrade Oliveira [1,5], Pietro Traversa [2,3,5], Guilherme Ferraz de Arruda [4] & Yamir Moreno [2,3]

The rapid spread of information and rumors through social media platforms, especially in group settings, motivates the need for more sophisticated models of rumor propagation. Traditional pairwise models do not account for group interactions, a limitation that we address by proposing a higher-order rumor model based on hypergraphs. Our model incorporates a group-based annihilation mechanism, where a spreader becomes a stifler when the fraction of hyperedges aware of the rumor exceeds a threshold. The dynamics has two distinct subcritical behaviors: exponential and power-law decay, which can coexist depending on the heterogeneity of the hypergraph. Interestingly, in the set of parameters we analysed, we found continuous phase transitions in both homogeneous and heterogeneous hypergraphs. This finding aligns with the literature suggesting that real-world rumor propagation occurs near criticality. Finally, we validated our model using empirical data from Telegram and email cascades, which provides additional evidence and possible explanations for this criticality claim. These results open the door to a more detailed understanding of rumor dynamics in higher-order systems.

Rumor and information propagation pose a challenge that increasingly demands systematic understanding as human communication scales up in volume and complexity, affecting various societal aspects. In particular, a significant part of this communication takes place in social media platforms, one of the main sources of contemporary information consumption[1]. As public referenda and elections require informed decisions from individuals and they turn to such platforms, they are targeted as fertile ground for misinformation campaigns and ideological polarization phenomena[2]. Adequate policies to regulate platforms need to be built from scientific knowledge, drawing from the mathematical modeling of mechanisms explaining the emergent collective behavior[3]. Although much of the empirical research on the spread of misinformation has been conducted on microblogging platforms[4,5], mobile messenger apps are widely used in populous countries such as India, Brazil, Nigeria, and Indonesia[6]. As a result, much of the understanding gained from network diffusion models may not be directly applicable to mobile messenger apps such as WhatsApp or Telegram. In these platforms, users are organized into groups, and the information is typically forwarded from group to group. Dyadic interactions are no longer sufficient to adequately describe the spread of group-mediated rumors, which means that mobile messenger apps are suitable objects for studying nonlinear dynamics through higher-order interactions[7].

Spreading processes on higher-order interactions constitute one of the latest research frontiers in network science, involving both contagion[8] and diffusion dynamics[9,10]. Compartmental models are featured in recent developments for both simplicial complex[11–15] and hypergraph[16–19]. For the latter, it has been recently proposed that the mechanism of changing social norms via critical mass[20] is behind rich phenomena on hypergraph contagion, such as multistability and hybrid phase transitions[12–14]. In this class of models, once a fraction of individuals in a group is infected, so are the remaining susceptible individuals in that same group. However, implementing a rumor-propagation annihilation process from the same principle remains unclear since to follow Daley–Kendall's original proposal[21], which was further adapted in the equally important Maki–Thompson model[22], the annihilation is to be produced from social interaction.

[1]Social Dynamics Research Lab, Department of Psychology, University of Limerick, Limerick, Ireland. [2]Institute for Biocomputation and Physics of Complex Systems (BIFI), University of Zaragoza, Zaragoza, Spain. [3]Department of Theoretical Physics, University of Zaragoza, Zaragoza, Spain. [4]Institute of Physics, Gleb Wataghin, University of Campinas (UNICAMP), Campinas, São Paulo, Brazil. [5]These authors contributed equally: Kleber Andrade Oliveira, Pietro Traversa. e-mail: yamir@unizar.es

We introduce a higher-order rumor model that follows threshold-based propagation, as in refs. 12–14, and incorporates group-based annihilation, whose definition is inspired by how rumors spread in messaging applications such as Telegram. Our model builds on the fundamental principle that rumor annihilation occurs through interaction with individuals who are already familiar with the rumor, rather than being spontaneous, following the original proposal of the Daley–Kendall model[21], but extending this idea to a group-structured population. We found a rich behavior depending on the propagation and annihilation thresholds, including regions of exponential or power-law decay to an absorbing state in the subcritical regime. The boundaries of these regions can be non-trivial in the presence of heterogeneity, including regions where both behaviors can coexist, depending on the initial condition. Importantly, we find empirical evidence for our model using a Telegram public channels dataset[23]. At the same time, our results may also provide a mechanistic explanation for the observation that real-world rumors occur near criticality, as proposed in ref. 24.

Results

Model definition

First, we define the hypergraph to represent group interactions in the rumor model. A hypergraph is a generalization of a graph in which edges connect not just two nodes but any number of nodes. These groups of nodes are called hyperedges, and the size of a hyperedge is called cardinality. Let $\mathcal{H}=\{\mathcal{V},\mathcal{E}\}$ be a connected hypergraph such that $\mathcal{V}=\{v_1,v_2,\cdots,v_N\}$ is the set of nodes, while $\mathcal{E}=\{e_1,e_2,\cdots,e_M\}$ is the set of hyperedges, where e_j is a subset of $\mathcal{V}$. To simplify the notation, we will always use i to index nodes and j to index hyperedges. The hypergraph structure is completely described by an incidence matrix $\mathcal{I}$, defined as

$$\mathcal{I}_{ij}=\begin{cases}1 \text{ if } v_i\in e_j,\\ 0 \text{ otherwise.}\end{cases} \tag{1}$$

It is also useful to define the degree of a node, $k_i=\sum_j \mathcal{I}_{ij}$, which corresponds to how many hyperedges it belongs to.

In a rumor model, node v_i can be in one of three states: (i) ignorant ($X_i=1$), individuals who are not aware of the rumor; spreader ($Y_i=1$), individuals who are aware of the rumor and spread it; and (iii) stifler ($Z_i=1$), individuals who are aware of the rumor but no longer spread it. We track their states with three associated Bernoulli random variables $X_i(t)$, $Y_i(t)$, and $Z_i(t)$. The three random variables are linearly dependent and must satisfy the condition $X_i(t)+Y_i(t)+Z_i(t)=1$. In addition, nodes change their states based on two types of processes: (i) the contagion process ($X\to Y$), in which ignorant nodes become spreaders, and (ii) an annihilation process ($Y\to Z$), in which spreaders become stiflers.

We model the contagion process as a higher-order contagion process with threshold dynamics, similar to[14]. The contagion is a Poisson process that occurs at a rate λ when the number of spreaders in a hyperedge reaches a certain threshold $\Theta_\lambda^{(j)}$. When this condition is met, all the ignorants in the hyperedge become spreaders, and we say that the hyperedge is activated. Mathematically, it is useful to introduce a random variable $T_j(t)$ that counts the number of spreaders at time t in a hyperedge e_j such that

$$T_j(t)=\sum_{i:v_i\in e_j} Y_i(t)=[\mathcal{I}_{\cdot j}]^T\mathbf{Y}(t), \tag{2}$$

where $[\mathcal{I}_{\cdot j}]$ is the j-th column of $\mathcal{I}$ and $\mathbf{Y}(t)$ is the vector of Bernoulli variables $Y_i(t)$ of size N and at time t. For each e_j, we compare $T_j(t)$ with $\Theta_\lambda^{(j)}$ to determine if the hyperedge can be activated.

Complementarily, we model the annihilation process as a node-based process with a threshold defined on the degree of the node. Let the annihilation be a Poisson process that occurs when the number of activated hyperedges v_i belongs to is above a certain threshold $\Theta_\alpha^{(i)}$. We can define a vector $\mathbf{B}(t)$ indexed by j such that it is 1 if e_j has already been activated by contagion at time t and 0 otherwise. Then we write the number of activated hyperedges to which v_i belongs as

$$S_i(t)=\sum_{j:v_i\in e_j}\prod_{\ell:v_\ell\in e_j}\left(1-X_\ell(t)\right)=\mathbf{B}^T(t)[\mathcal{I}_{i\cdot}]^T, \tag{3}$$

where the summation runs over all hyperedges to which node v_i belongs, $X_\ell(t)$ tracks which neighboring nodes of v_i are ignorant at time t, and $[\mathcal{I}_{i\cdot}]$ is the i-th row of the incidence matrix. Note that, by definition, an activated hyperedge cannot contain ignorant nodes.

To avoid a cumbersome notation, from this point on, we drop the explicit dependence on time of $X_i(t)$, $Y_i(t)$, $T_j(t)$, and $S_i(t)$. Thus, under these assumptions, the equation describing the time evolution of the probability of node v_i being a spreader is given by

$$\frac{d\langle Y_i\rangle}{dt}=\left\langle \lambda X_i\sum_{j:v_i\in e_j}H(T_j-\Theta_\lambda^{(j)})-\alpha Y_i H(S_i-\Theta_\alpha^{(i)})\right\rangle, \tag{4}$$

where $\langle\cdot\rangle$ is the expectation operator, $H(x)$ is the Heaviside function which is zero for $x<0$ and 1 for $x\geq 0$, and the terms $\Theta_\lambda^{(j)}$ and $\Theta_\alpha^{(i)}$ can depend on the hyperedge e_j or the node v_i. In particular, we focus our study on the case where contagion is controlled by $\Theta_\lambda^{(j)}=\lfloor(\Theta_\lambda\times|e_j|)\rceil$ and annihilation is controlled by $\Theta_\alpha^{(i)}=\lfloor(\Theta_\alpha\times k_i)\rceil$, where k_i is the degree of the node v_i. In this way, Θ_λ and Θ_α are numbers between 0 and 1 that can be fixed independently of hyperedge cardinalities and degrees. The function $\lfloor x\rceil$ rounds x to its nearest integer. This choice is motivated by the intuition that the larger a group is, the harder it is to inform all group members. Similarly, for annihilation, the more groups one participates in, the more reluctant the spreader is to become a stifler.

To analyze our model, we focus on the time to reach an absorbing state, τ, and the fraction of individuals reached by the rumor, $z=\langle Z\rangle$. We rely on Monte Carlo simulations performed by the Gillespie algorithm described in the section "Methods." Both τ and z are estimated using an average over n_{sim} simulations, which can vary depending on the experiment. Figure 1A illustrates the rich behavior observed in terms of regimes for different combinations of the two thresholds, where we can identify four regions:

(I) Fig. 1B, E. A region whose subcritical regime decays exponentially into an absorbing state, i.e., $\tau\propto\exp(-\alpha)$, which is the same subcritical behavior as an SIS or an SIR on a graph[25,26] (note that τ peaks at the critical point);
(II) Fig. 1C, F. A region whose subcritical regime decays as a power-law to an absorbing state, i.e., $\tau\propto\lambda^{-1}$, which is the same subcritical behavior as the Maki–Thompson model on a graph[27] (note that τ is the largest at the smallest λ);
(III) Fig. 1D, G. An active region where the rumor is always in the supercritical regime (note that for a non-zero λ, even when $\lambda\to 0$, $z>0$, and that a change in the derivative of z is present, but there is no phase transition);
(IV) An inactive region where the rumor does not spread.

The active and inactive regions are separated by $\Theta_\lambda{}^1$, below which the process is active, while above which the process cannot start because there are not enough spreaders to trigger the spreading. The three active regions are separated by the boundaries $\Theta_\alpha{}^1$ and $\Theta_\alpha{}^2$ (see Fig. 1A). The threshold $\Theta_\alpha{}^1$ marks the regime where, below it, every node in the hypergraph recovers exponentially fast, provided the rumor is able to spread, while $\Theta_\alpha{}^2$ is the value above which the rumor always reaches a non-zero fraction of the population, even for small but non-zero λ.

Two mechanisms explain the subcritical behavior in regions (I) and (II). In (I), the exponential behavior is due to a low annihilation

https://doi.org/10.1038/s41467-026-70096-w

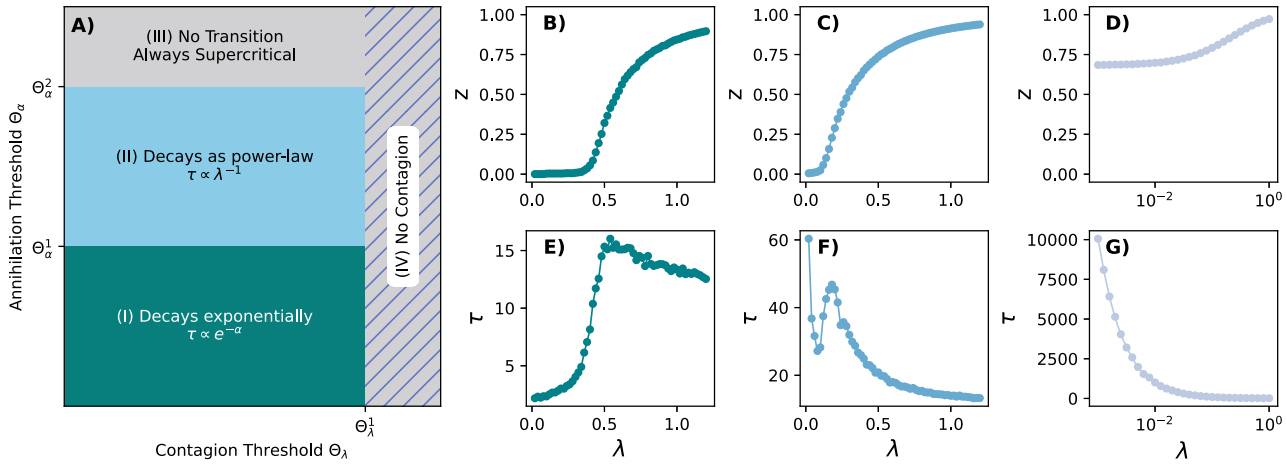

Fig. 1 | Phase diagram of the hypergraph rumor model. A Schematic representation of the critical and subcritical behavior depending on the annihilation and contagion threshold parameters. If the contagion threshold is too high, no contagion is possible. If the annihilation threshold is low, each active node can recover exponentially fast, and the time to the absorbing state, τ, also decays exponentially with rate α. As the annihilation threshold increases beyond a certain value, some spreading processes must occur to trigger the recovery processes, and thus, the absorbing time decreases as a power law as λ^{-1}. **B**, **E** The order parameter and the absorption time in the exponential regime, respectively. This example was generated with $\Theta_\alpha = 0.09$ and $\Theta_\lambda = 0.3$. **C**, **F** The order parameter and the absorption time in the power-law regime, respectively, with $\Theta_\alpha = 0.4$ and $\Theta_\lambda = 0.35$. Finally, **D**, **G** The order parameter and absorbing time in the case where the rumor always reaches a fraction of the population, so there is no transition. For this regime, we chose $\Theta_\alpha = 0.5$ and $\Theta_\lambda = 0.2$. All examples are run on the same hypergraph with truncated Poisson-distributed cardinalities and degrees, i.e., $P(k) = \frac{1}{1-e^{-\nu}-\nu e^{-\nu}}\frac{\nu^k e^{-\nu}}{k!}$, for $k \geq 2$ and $\nu = 2$ (similarly for $|e|$), leading to an average of approximately 2.9.

threshold where the initial condition is sufficient to trigger the process. Thus, since the events are modeled by Poisson processes, the expected time for the next annihilation event is exponential with the parameter α. On the other hand, in region (II), the power-law behavior is a consequence of a moderately high threshold and of $\alpha \gg \lambda$. In this case, we need at least one spreading event to reach the absorbing state, which takes, on average, λ^{-1} time units. Note that these mechanisms are fundamental for describing the subcritical regime, but both coexist in the supercritical regime.

Evaluating the bounds ${\Theta_\lambda}^1$, ${\Theta_\alpha}^1$, and ${\Theta_\alpha}^2$ is challenging, as they generally depend on the degree and cardinality distributions of the hypergraph. However, we can give some bounds independent of the distributions (see the section "Methods" for their derivations), and we get

$$ {\Theta_\alpha}^1 = \frac{1}{k_{\max}}, \; {\Theta_\alpha}^2 = \frac{1}{k_{\min}}, \tag{5} $$

where $k_{\min}$ and $k_{\max}$ are the minimum and maximum degrees, respectively. Similar considerations lead to the evaluation of the inactive region as

$$ {\Theta_\lambda}^1 = 1 - \frac{1}{|e|_{\max}}. \tag{6} $$

We note that ${\Theta_\alpha}^1$ and ${\Theta_\alpha}^2$ define the extreme regions of this parameter space, i.e., (I) and (III), while the intermediate region can be a mixture of both behaviors, which can coexist for heterogeneous degree distributions. More specifically, since the rumor model has infinitely many absorbing states in the thermodynamic limit, in the subcritical regime, the process depends only on the initial conditions. In our simulations, we define the initial condition by randomly selecting a single hyperedge and setting all its nodes as spreaders. In this case, these bounds can be interpreted in terms of the degrees of the nodes in this hyperedge. Replacing $k_{\max}$ and $k_{\min}$ by $k_{\max}^{(j)} = \max_{v_i \in e_j} k_i$ and $k_{\min}^{(j)} = \min_{v_i \in e_j} k_i$ of the nodes in the initially activated hyperedge, e_j, in the previous expression (5) will give us a new set of conditions. Figure 2

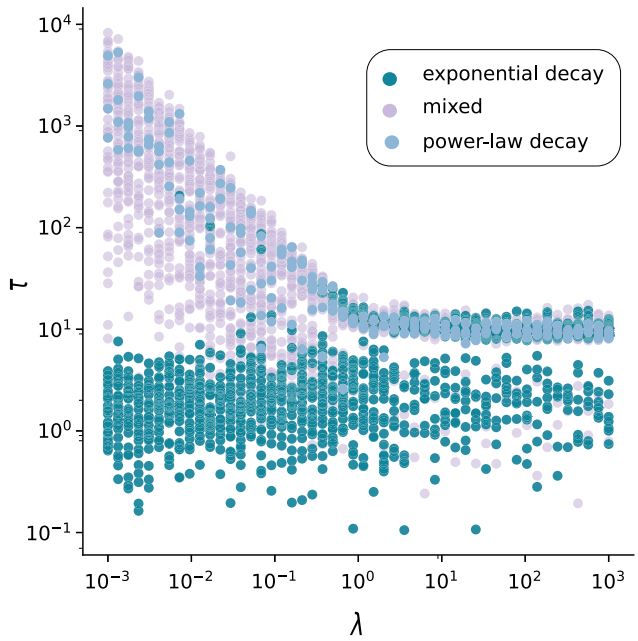

Fig. 2 | Dependence of the subcritical regimes on the initial condition. We show the absorption time τ as a function of λ for different initial conditions. Simulations labeled as "exponential decay" have initial conditions satisfying $k_i \times \Theta_\alpha \leq 1 \; \forall \; i$: $v_i \in e_j$, where e_j is the initially infected hyperedge. In the subcritical regime, these initial conditions necessarily lead to exponential decay. Instead, the initial conditions of the "power-law decay" simulations satisfy $k_i \times \Theta_\alpha > 1 \; \forall \; i$: $v_i \in e_j$. In these cases, a contagion process is forced to occur, leading to a power-law decay. The solutions labeled as "mixed" are those where we have different nodes satisfying different conditions. We considered a hypergraph with $N = 10^4$ nodes, and both degree and cardinality follow power-law distributions as $P(k) \sim k^{-\gamma}$ and $P(|e|) \sim |e|^{-\gamma}$ with $\gamma = 2.3$, with $k_{\min} = 2$ and $k_{\max} = 100$. The simulation parameters are $\Theta_\alpha = 0.1$, $\Theta_\lambda = 0.5$, and we run $n_{\text{sim}} = 10^2$ independent simulations (initial conditions) for each value of λ. The critical point is around $\lambda_c \approx 0.12$.

https://doi.org/10.1038/s41467-026-70096-w

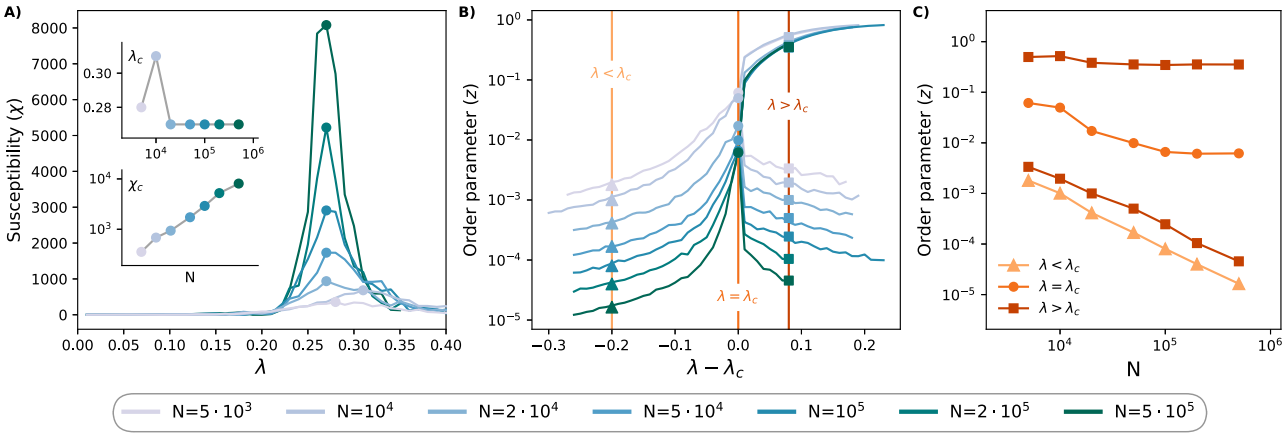

Fig. 3 | Finite-size analysis on a homogeneous hypergraph. We show the dependence of the susceptibility (**A**) and the order parameter (**B**, **C**) on the system size. Using the peak of the susceptibility, we identify the critical point and show that it converges to the value $\lambda_c = 0.27 \pm 0.01$. The order parameter is plotted as a function of N in (**C**) to highlight the subcritical regime, which scales as N^{-1}, the critical regime, which also goes to zero but sublinearly, and the supercritical regime. The latter has two branches, one independent of N and one that scales as the subcritical regime. The synthetic hypergraph was generated with a cardinality and degree sequence distributed according to a truncated Poisson for $k \geq 2$, and $|e| \geq 2$ with $\nu = 4.0$, leading to an average degree and average cardinality of approximately 4.3. We ran $n_{sim} = 10^3$ independent simulations with the following parameters: $\Theta_\lambda = 0.3$, $\Theta_\alpha = 0.2$, and we used $N^{-\frac{1}{2}}$ as the threshold for computing the susceptibility (see the section "Methods" for details).

illustrates the dependence of the subcritical regimes on the initial condition of heterogeneous hypergraphs. Note, however, that region (II) does not exist for a uniform and regular hypergraph since both bounds are the same, but this region does exist for non-regular and non-uniform systems.

Numerical analysis

To study the transitions in our model, we perform a finite-size analysis for a homogeneous hypergraph. Here, we refer to homogeneous hypergraphs as hypergraphs with both degree and cardinality distributions following a truncated Poisson distribution. In Fig. 3A, we show the susceptibility, defined as $\chi = N \times \left(\langle Z^2 \rangle - \langle Z \rangle^2\right) \times \langle Z \rangle^{-1}$, as the number of nodes increases. The peak of the susceptibility curve indicates the critical point, which converges to a value around $\lambda_c = 0.27 \pm 0.01$. In addition, the peak of the susceptibility, χ_c, approximately follows $\chi_c \sim N^{0.68}$ (see the inset in Fig. 3A). Complementarily, Fig. 3B, C shows the scaling of the order parameters, highlighting the subcritical behavior, $\lambda < \lambda_c$, the critical point, $\lambda = \lambda_c$, and the supercritical behavior, $\lambda > \lambda_c$. The subcritical behavior of the order parameter scales as $z(\lambda < \lambda_c) \sim N^{-1}$ since the size of the rumor is limited to the initial set of infected nodes or a very small fraction of the active nodes. At the critical point, the average fraction of stiflers tends to zero as $z(\lambda_c) \sim N^{-0.56}$, which is slower than the subcritical scaling. Finally, the supercritical regime consists of two branches, one in which $z(\lambda > \lambda_c) \sim O(1)$, the active state, and another that follows $z(\lambda > \lambda_c) \sim N^{-1}$. Note that even if the propagation rate is large enough for a microscopic initial state, there is a non-zero probability that the rumor will die out before reaching a macroscopic state. This is a consequence of the stochastic nature of the process. Note that this probability also decays as λ increases.

Figure 3 A, B shows that the observed phase transitions are continuous. This observation was also confirmed by additional simulations in homogeneous, heterogeneous, and real hypergraphs (see Supplementary Section S2 for additional results). Interestingly, this result contrasts with the social contagion model in refs. 12,14, where the transitions are expected to be hybrid[14]. Along the same lines, many spreading models in higher-order networks predict discontinuous transitions[8]. Indeed, in the simplicial contagion[11], the quenched mean-field approximation predicts that to have a continuous phase transition, we must also have enough pairwise connections to drive such a transition[28]. This suggests that the continuous phase transition may be related to the structure, the parameters evaluated, and their interplay with the annihilation mechanism, which depends on the interaction with other individuals rather than on spontaneous transitions, as in the models mentioned above. This argument was used by the authors in ref. 29, who proposed a higher-order healing mechanism for contagion (SIS) dynamics, where both spreading and healing depend on the product of the states of the neighbors. In this case, only continuous transitions were observed.

In general, obtaining the phase diagram for real rumor processes is challenging, if not inaccessible. This is because it is not possible to know exactly when a person becomes a stifler, as the process is inherently related to the person's loss of interest in spreading the news or rumor further. Thus, to compare results from numerical simulations and real rumor propagation, we should use measurable observables for both synthetic and real rumor spreading. Next, we focus on two of such observables: rumor cascade sizes and their survival times. Defining cascades in rumor dynamics is also demanding, but can be done from the content of messages and their time stamp (e.g., mobile messenger datasets). This can be used as a probe for spreading events. In Fig. 4, we show results for our rumor model on synthetic heterogeneous hypergraphs. Note that different hypergraphs with the same parameters will not result in the same regime. Therefore, to remain in a regime with mixed subcritical behavior, we use different thresholds with respect to the homogeneous case in Fig. 3. For more details on how the distributions impact the model's regime and critical point, see Supplementary Figs. 3 and 4. Figure 4A, B represents how the survival time changes as a function of the average inter-event time for different values of λ and cascade size, respectively. Results are reported for $\lambda \in [10^{-6}, 10^{1}]$, which covers all regimes. We find the transition point to be around $\lambda_c = 0.4$, as highlighted in the inset of Fig. 4A. The critical point is shown with a dotted line and corresponds to the average of the region where two distinct branches begin to appear. The supercritical regime is the upper branch after the critical point. In this case, the cascades reach a macroscopic fraction of the population, whereas, as expected for second-order phase transitions, the variability of the cascade sizes around the critical point is high.

Empirical evidence: the Pushshift Telegram dataset

To validate our model, we use real examples of rumor propagation in higher-order systems. Mobile messenger apps allow data collection with time stamps, i.e., it is possible to know exactly the time at which

https://doi.org/10.1038/s41467-026-70096-w

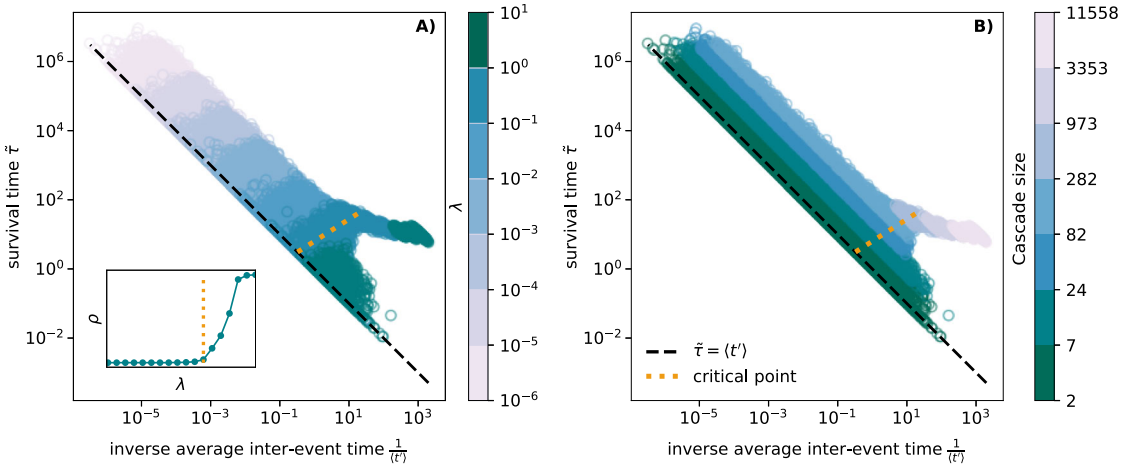

Fig. 4 | Analysis of simulated inter-event time on a heterogeneous hypergraph. We estimate the average inter-event time and the survival time for the hypergraph rumor model on a heterogeneous hypergraph simulating different contagion rates. In (**A**), we show the different behavior below and above the transition point. We also show the phase transition and the critical point in the inset. In (**B**), we show the sizes of the cascades. We consider the time points to be the moment at which a contagion process occurred. We discard the annihilation processes from the time series because they are not observable in real scenarios. We considered a hypergraph with $N = 10^4$ nodes, and both degree and cardinality follow power law distributions as $P(k) \sim k^{-\gamma}$ and $P(|e|) \sim |e|^{-\gamma}$ with $\gamma = 2.3$. The simulation parameters are $\Theta_\alpha = 0.08$, $\Theta_\lambda = 0.5$, and we run $n_{\text{sim}} = 10^3$ independent simulations for each value of λ.

messages are sent, which is equivalent to rumor activity in our problem. This allows us to track each contagion process in time and define a cascade of contagion events. We can also know when the last message on a particular topic was sent and identify that moment as the time when the rumor died out. This provides an estimate of the rumor's absorption time.

To compare the behavior of our model with real-world rumor dynamics, we analyze the Pushshift Telegram dataset[23] (see the section "Methods" subsection "Pushshift Telegram dataset and hypergraph construction" for details). We identify a rumor as messages containing a fixed Uniform Resource Locator (URL), which allows us to construct a cascade of messages and compute the corresponding average time between events. Additionally, we measure the survival time of a rumor as the time elapsed between the first and the last time it was sent. The average inter-event time and survival time for each cascade are shown in Fig. 5A.

Furthermore, in Fig. 5B, we show the simulated cascades in the telegram hypergraph. We use a contagion threshold of $\Theta_\lambda = 0.1$ in the simulation based on an estimate derived from the intersection of the Telegram groups (see the section "Methods" subsection "Pushshift Telegram dataset and hypergraph construction"). As it is not possible to estimate the annihilation threshold from the data, we have set $\Theta_\alpha = 0.01$, corresponding to a regime where both exponential and power-law decay are present. In particular, we focus on values of λ around the critical point since this is the region where the cascades most closely resemble the real case. Note the similarities between the real and simulated cascades shown in Fig. 5. Given that the model is Markovian, one could rescale the rates in the simulation so that they are in similar ranges to the real data. We chose these rates to avoid numerical problems. It should also be noted that the real case does not have the supercritical branch, while our simulation does. The fact that rumors in the Telegram dataset form cascades that fall into subcritical and critical behavior is in accordance with[24]. Importantly, Fig. 5 shows that our model captures the cascade behavior in the real data.

To strengthen this claim, we provide an additional way to compare the empirical distributions and their simulated counterparts. However, we want to highlight that it is complicated to perform a rigorous analysis due to the complexity of the parameters and the unknowns in the data. For example, all the recovery processes are unobservable, since we cannot exactly know the time a user becomes a stifler. Additionally, the basic assumption behind comparing cascades is that the real process is Markovian (memoryless), which is not necessarily true.

With these limitations in mind, we perform a quantitative analysis by computing the difference between the real cascade size distribution and the cascade size distributions obtained by simulating our model at different values of λ. To quantify this difference, we use the ratio between the mean and the variance of the distribution (see "Methods" subsection "Mean-Variance ratio difference"). The intuition behind this choice is that, in the subcritical regime, we expect the distribution of cascade sizes to conform to an exponential, while in the critical regime, it would approach more of a power-law. Therefore, the ratio should capture the moment when the distribution changes its character. Fig. 6 shows how this ratio varies as the parameter λ used in the simulation changes. The minimum difference between the real and simulated cascade size distributions is obtained close to the critical point λ_c, i.e., the value of λ for which the susceptibility is maximal.

Thus, the similarities between our simulations and the real data provide additional evidence that rumors spread around criticality in real scenarios, again consistent with the findings in ref. 24. Complementarily, Supplementary Figs. 5 and 6 show the results for the email dataset[30]. As can be seen, we obtained similar results, confirming our previous findings.

Discussion

We have introduced a higher-order rumor model that incorporates group-based annihilation, which follows the original proposal of the Daley–Kendall model[21], i.e., that rumor annihilation occurs through interaction with individuals who are already familiar with the rumor. Additional motivation for our threshold-based annihilation approach can be found in ref. 31. Although the ideas in ref. 31 were motivated by contagion, activation was proposed as a process associated with individuals, similar to our approach.

To our knowledge, the first higher-order healing mechanism in the context of higher-order networks was proposed in ref. 29, where the motivation was that if a trend is popular in groups, then this might make individuals less likely to adopt such a trend. They also called this the "hipster effect." Although this mechanism is similar to annihilation in rumor spreading, the model proposed in ref. 29 still

https://doi.org/10.1038/s41467-026-70096-w

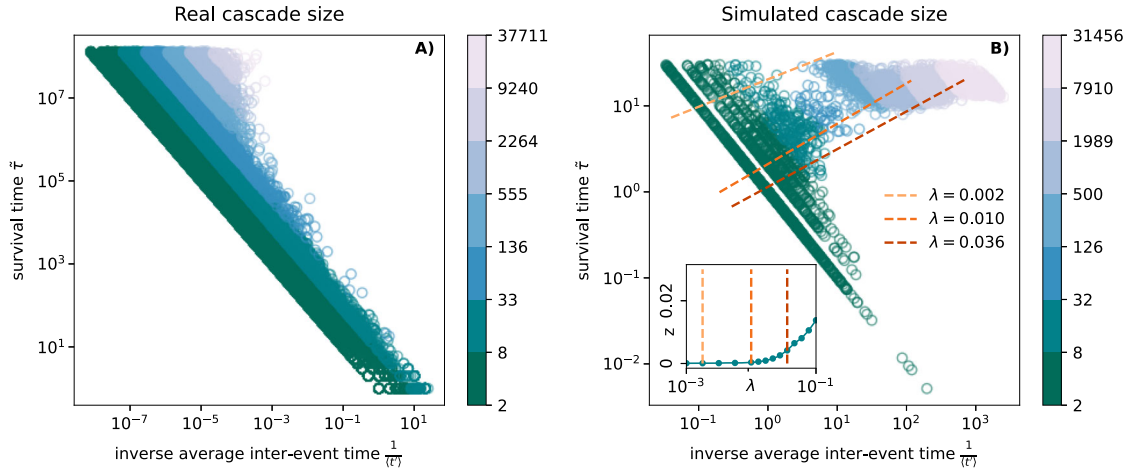

Fig. 5 | Comparison between real observed and simulated cascades. In (**A**), we plot the survival time versus the inverse of the average inter-event time for the observed cascade of Telegram messages forwarded from one group to another. For this calculation, we only considered messages containing a URL. In the main panel of (**B**), we show simulated cascades on the Telegram hypergraph using the rumor model with parameters $\alpha = 1$, $\Theta_\lambda = 0.1$, $\Theta_\alpha = 0.01$, and $n_{\text{sim}} = 10^3$ independent simulations for each value of λ. The simulation is plotted with a cutoff on the survival time to replicate the real behavior, in which we can observe cascades up to a certain time. The inset of (**B**) features a phase transition for the order parameter z versus the control parameter (contagion rate) λ. Note that the simulations shown in (**B**) are generated using a range of λ close to the critical point. Furthermore, the discrepancy in time scale between the real and simulated cases is not an issue since the parameter α in the simulations can be adjusted accordingly to rescale the time.

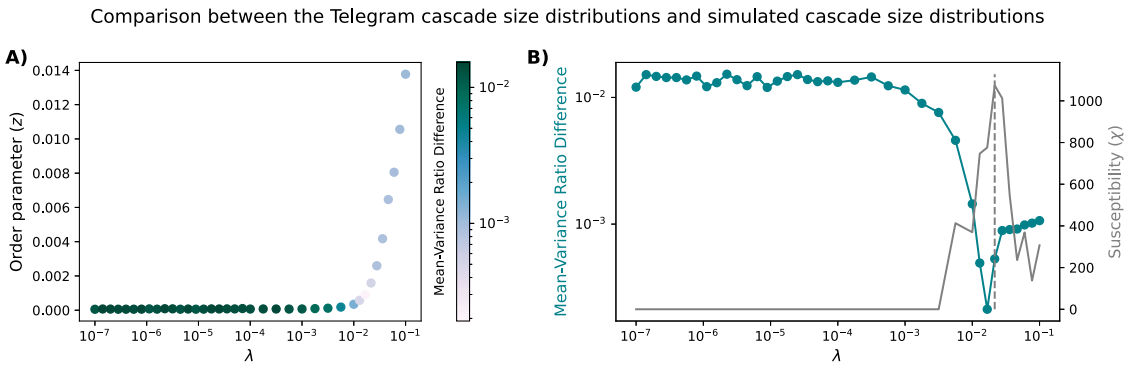

Fig. 6 | Mean-variance ratio difference between the Telegram cascade size distribution and the simulated ones. We show that the real cascade size distribution generated from the telegram dataset is similar to the one obtained by simulating our model when the spreading rate λ is close to criticality. **A** The order parameter, with each λ colored according to the value of the difference $|r_{\text{real}} - r_{\text{sim}}(\lambda)|$, where r is the ratio between the average and the variance of the cascade size distribution. In (**B**), on one y-axis, we show the value of the comparison metric $|r_{\text{real}} - r_{\text{sim}}(\lambda)|$ and the susceptibility on the other y-axis. The critical point λ_c corresponds to the point where the susceptibility is maximal and is highlighted by a dashed line. It can be seen that this point is very close to the point where the difference between the real and simulated mean-variance ratio is minimal. The simulations parameter are $\alpha = 1$, $\Theta_\lambda = 0.1$, $\Theta_\alpha = 0.01$, and $n_{\text{sim}} = 10^3$ for each λ.

has a single absorbing state and is intended to be an extension of the SIS model.

In addition, as future work, exploring alternative versions of higher-order annihilation may be useful in other rumor-spreading contexts, especially when the cardinality of the hyperedge is small, and it becomes more reasonable for a spreader to track the state of individual nodes rather than entire groups. An interesting open question, then, is how different annihilation processes shape the dynamics and whether these models can be unified into the same class.

Our model has two different subcritical behaviors, exponential or power-law decay to an absorbing state. Interestingly, the exponential decay resembles the behavior of an SIR model in a graph[25,26], while the power-law decay has been observed in the Maki–Thompson rumor model[27]. The main mechanism behind this variety of behavior is the threshold-based annihilation process, which is higher-order by definition. If the threshold is low enough, the subcritical behavior is exponential because the initial condition is sufficient to trigger its own annihilation process, similar to a spontaneous process. Note that this happens regardless of the propagation rate. On the other hand, if the threshold is moderately high and $\lambda \ll \alpha$, at least one spread must occur for the annihilation threshold to be reached. This produces a power-law behavior of the form $\tau \propto \frac{1}{\lambda}$ similar to the subcritical behavior of the Maki–Thompson model.

In heterogeneous systems, which is the case of many real systems, both behaviors can be observed depending on the initial condition. In fact, the parameter space in Fig. 1A changes slightly in the presence of heterogeneity. In particular, for a power-law hypergraph with $P(k) \sim k^{-2.3}$ and $P(|e|) \sim |e|^{-2.3}$, we observed that the "always supercritical" region becomes larger while the power-law decay region becomes smaller (see Supplementary Section S2 for more details). Moreover, the analysis of the subcritical behavior of our model is particularly interesting because the Maki–Thompson and SIR models have traditionally been studied separately. By incorporating these behaviors into a single framework, our model opens up new avenues of investigation. Future

work can focus on rigorously calibrating the model to real-world scenarios and determining whether a dominant annihilation process emerges or whether a mixed effect occurs naturally.

Regarding the critical behavior, we first highlight that it is common to observe discontinuous phase transitions in dynamical processes occurring on top of higher-order networks[8]. In our numerical analysis, however, we observed only continuous phase transitions. The main differences between our model and the social contagion counterpart proposed in ref. 12 are the number of absorbing states and the annihilation mechanism. Regarding the former, continuous transitions were also found in higher-order SIR dynamics on simplicial complexes[32]. Only in the presence of strong heavy tails in the distribution of groups of size 3, the authors observed a continuous transition followed by an abrupt one. Although our model is different from the simplicial SIR, both share the property of having infinitely many absorbing states in the thermodynamical limit. Notably, our model becomes comparable with an SIR-like dynamics in the limit of $\Theta_\alpha = 0$. We have performed a finite-size analysis for this case, and we only observed continuous transitions, see Supplementary Fig. 7. Additionally, in ref. 29 discontinuous transitions were not found either, which provides evidence that the continuous phase transitions of our model are also related to the non-spontaneous annihilation. Along similar lines, another relevant question would be whether it is possible to have discontinuous transitions in our model, either hybrid as in refs. 12,14 or purely first-order. In this case, what would be the sufficient and necessary conditions for such behavior? The formal verification of these questions is an open problem.

Despite the nature of the transition, the critical point changes as a function of both the structure and the contagion and annihilation thresholds. The interplay between these quantities is not trivial. Indeed, we found that the region of the parameter space $\Theta_\lambda \times \Theta_\alpha$ in which a phase transition is observed is significantly smaller for power-law hypergraphs than for the truncated Poisson hypergraphs (see Supplementary Section S2 for additional experiments). Understanding the interplay between the structure and the contagion and annihilation thresholds is another open problem.

Finally, we stress that our results are consistent with the existing literature and provide evidence that real-world rumor spreading tends to occur near criticality[24]. By comparing message cascades in Telegram with our simulations, we found that the contagion rate at which the cascades align is close to criticality. To the best of our knowledge, this is the first attempt to compare empirical observations of an unknown underlying dynamical process with a spreading model of this class on hypergraphs. Typically, higher-order spreading studies contrast empirical hypergraph structures with synthetic dynamical processes that generate artificial event times rather than using empirical event timestamps. We repeated the experiment with the email dataset[30] and obtained similar results (see Supplementary Section S3). Moreover, our model may provide a mechanistic explanation for the cascades observed in the real data, as it is able to reproduce some of their main features. To further validate this hypothesis, more real-world examples of rumor spreading and controlled experiments in higher-order systems need to be considered.

Methods

Gillespie algorithm

We simulate the rumor model using continuous-time Monte Carlo simulations via the Gillespie algorithm[33]. At each step, we track all contagion and annihilation processes that meet their respective thresholds and trigger them according to random samples from exponential distributions. Each process is a Poisson process parameterized by λ (contagion) or α (annihilation). The threshold parameters $\Theta_\lambda, \Theta_\alpha \in (0, 1)$ are evaluated in each process by rounding their product with the hyperedge cardinality (for contagion) or node degree (for annihilation). When a process is triggered, it updates node states and may abort pending processes (e.g., nodes transitioning to stiflers reduce the contagion threshold count).

The algorithm is initialized on a hypergraph where all nodes are ignorant except those in a single randomly chosen hyperedge, which are initialized as spreaders. The algorithm terminates when no more transitions are possible, typically when all spreaders become stiflers. However, in some cases, due to the annihilation threshold condition, a few spreaders may remain active at the end. While we did not perform a mathematical evaluation of the algorithm's complexity, we expect it to be similar to the standard Gillespie algorithm, which is of order $\mathcal{O}(N^2)$ for the SIR on pairwise graphs[34] and for the SIS on hypergraphs[35], where N is the system size. Although it is possible to speed up the calculation to order $\mathcal{O}(N)$ implementing a framework similar to[35], it was not necessary for the simulations in this paper. The code is provided in ref. 36.

To characterize the transition, we denote as Z^s the total number of stiflers at the end of simulation s, then the order parameter z is given by

$$z = \langle Z \rangle = \frac{1}{N}\left(\frac{1}{n_{\text{sim}}}\sum_{s}^{n_{\text{sim}}} Z^s\right), \tag{7}$$

where $\langle\cdot\rangle$ is the expectation operator, n_{sim} is the number of simulations. Then, we can define the susceptibility as

$$\chi = N\frac{\langle Z^2\rangle - \langle Z\rangle^2}{\langle Z\rangle}, \tag{8}$$

and we find the critical point λ_c as

$$\lambda_c = \text{argmax}_\lambda \chi. \tag{9}$$

Even above the critical point, some simulations may end with only a small number of stiflers due to stochastic fluctuations and the presence of thresholds. This effectively creates two branches: the upper critical branch and an inactive branch caused by randomness. If both branches were included, the calculated susceptibility would be significantly overestimated. To mitigate this problem, when calculating the susceptibility and the order parameter, we only consider simulations where the final number of stiflers satisfies $Z/N > N^{-\frac{1}{2}}$. If no simulations fulfill this criterion, the system is classified as subcritical, and all simulation calculations are included.

Synthetic hypergraphs

We simulate our model on synthetic hypergraphs with truncated Poisson and power-law degree and cardinality distributions. To generate the hypergraphs, we used an algorithm based on three steps: (i) an unrestricted matching, (ii) a brute-force fixing algorithm that swaps repeated nodes on the hyperedges, and (iii) a random swap step (using the swap proposed in ref. 37) that ensures that the final hypergraph is uniformly sampled from the space of possible hypergraphs. We perform 10^4 swaps for each hypergraph. This algorithm has been proposed, systematically tested, and used to generate hypergraphs in ref. 38. This algorithm can generate hypergraphs with the desired number of nodes, cardinality, and degree distribution, and it can also fix the maximum and minimum degree and cardinality. The distributions are truncated, and we choose the minimum degree $k_{\text{min}} = 2$ and the maximum degree $k_{\text{max}} = \sqrt{N}$, while the minimum cardinality $|e|_{\text{min}} = 2$ and the maximum cardinality $|e|_{\text{max}} = \sqrt{N}$.

Pushshift Telegram dataset and hypergraph construction

We studied the rumor propagation model using the Pushshift Telegram dataset[23]. This dataset contains 317,224,715 messages from 2,200,040 users. First, we build a hypergraph that maps each public channel and/or group identifier (ID) listed in each message's metadata to a hyperedge and each user ID to a node.

Since about 8.1% of the more than 317 million messages are forwarded from group to group, we use this information, whenever available, to assign the hyperedge membership of the user who posted the message to both groups. This results in a first partial reconstruction of the telegram hypergraph with 141,824 nodes and 143,343 hyperedges.

We then do the same with the rest of the messages, which only contain the ID of the group that received the message and attribute the one-way hyperedge membership to the posting user. Adding this new information to the existing hypergraph results in a total of 2,200,040 nodes and 143,501 hyperedges. Finally, we keep only the largest connected component of this hypergraph, which comprises almost all of its size. The resulting hypergraph is examined in the section "Results" subsection "Empirical evidence: the Pushshift Telegram dataset," which has 2,199,885 nodes and 143,475 hyperedges.

As shown in Supplementary Fig. 1, the hypergraph has heavy-tailed distributions for both cardinalities and degrees. The average cardinality is 22.14, but the 100 largest groups have at least 6088 members (up to a maximum of 61,377). In terms of degrees, users are connected to 1.44 groups on average, and the 100 largest degrees range from 217 to 2035. However, groups are able to connect many users simultaneously, which means that each user has 12,057 neighbors on average.

Importantly, the message IDs present in the metadata do not uniquely identify messages across the dataset but only within each group. For this reason, we build cascades of information sharing across groups by tracking URLs instead, since we can then say that it is the same rumor that is spreading throughout the system. Sent messages that contain the same URL are assumed to be about the same rumor. There are 2,314,550 unique URLs that appear in at least two messages in the dataset. Once a URL is fixed, we define a cascade as the ordered time series containing the time when messages containing that URL were sent from one group to another.

The data allows us to roughly estimate the value of the contagion threshold as $\Theta_\lambda \approx 0.1$. To do this, we select all messages containing a URL for which we have information about the sending and receiving groups and then compute the intersection of the two groups, normalized by the size of the sending group. This estimation is based on the idea that for one hyperedge to trigger another, it must share as many nodes with the next hyperedge as required by Θ_λ. The results are shown in the Supplementary Fig. 2.

Inter-event time analysis

Given a cascade $\{t_0, t_1, \ldots, t_s\}$ of size $s+1$, we measure the survival time $\tilde{\tau}$ as

$$\tilde{\tau} = t_s - t_0, \tag{10}$$

and average inter-event time $\langle t' \rangle$ as

$$\langle t' \rangle = \frac{1}{s}\sum_{i=0}^{s-1}(t_{i+1} - t_i) = \frac{t_s - t_0}{s} = \frac{\tilde{\tau}}{s}. \tag{11}$$

Mean-variance ratio difference

In the section "Results" subsection "Empirical evidence: the Pushshift Telegram dataset," we compared two distributions by using the ratio between their mean and their variance. Specifically, from the real cascades, we computed the average cascade size $\langle s_{\text{real}} \rangle$ and the variance σ^2_{real}. The ratio $r_{\text{real}} = \frac{\langle s_{\text{real}} \rangle}{\sigma^2_{\text{real}}}$ is what we are comparing with the simulated cascades.

We use the Telegram hypergraph to simulate our model and generate cascades of rumors for different values of λ. In particular, we considered 38 different values of $\lambda \in [10^{-7}, 10^{-1}]$, logarithmically spaced. For each of these λ, we can compute the average cascade size $\langle s_{\text{sim}}(\lambda) \rangle$ and variance $\sigma^2_{\text{sim}}(\lambda)$, to get the ratio $r_{\text{sim}}(\lambda) = \frac{\langle s_{\text{sim}}(\lambda) \rangle}{\sigma^2_{\text{sim}}(\lambda)}$.

Finally, we define the mean-variance ratio difference as $|r_{\text{real}} - r_{\text{sim}}(\lambda)|$. The value of λ for which this difference is minimal corresponds to when the real and simulated distributions are more similar.

Derivation of threshold bounds

In the "Results" subsection "Model definition," we introduced three bounds that separate the regimes shown in Fig. 1A. The first bound, ${\Theta_\alpha}^1$, represents the threshold below which every node in the hypergraph recovers exponentially fast, provided the rumor spreads. In this regime, a spreader node becomes a stifler as soon as it belongs to a single active hyperedge. Mathematically, this corresponds to the condition where the term $Y_i H(S_i - k_i \Theta_\alpha)$ in Eq. (4) is equal to 1 for all i. In order to recover, $Y_i = 1$, implying that at least one hyperedge is active. Then $S_i \geq 1$, leading to the condition that if

$$\Theta_\alpha \leq {\Theta_\alpha}^1 = \frac{1}{k_{\max}}, \tag{12}$$

where $k_{\max}$ is the maximum degree, all nodes recover exponentially fast. In this regime, the model behaves similarly to an SIR model with critical mass contagion.

Conversely, ${\Theta_\alpha}^2$ is the value above which the rumor always reaches a finite fraction of the population, even for an arbitrarily small but positive λ. Estimating this bound is more complex since it also depends on Θ_λ (see Supplementary Section S2 for an example). However, we can give an upper bound as

$$\Theta_\alpha > {\Theta_\alpha}^2 = \frac{1}{k_{\min}}, \tag{13}$$

where $k_{\min}$ is the minimum degree.

Finally, there is an inactive region above the value ${\Theta_\lambda}^1$, where the rumor never reaches a finite fraction of the population. This happens when the term $X_i H(T_j - |e_j|\Theta_\lambda)$ in Eq. (4) is always 0 for each hyperedge e_j. To be infected, $X_i = 1$, implying that the sum of infected nodes in a hyperedge e_j is bounded by $T_j < |e_j| - 1$. Thus, any $\Theta_\lambda > (|e_j| - 1)/|e_j|$ makes the contagion of hyperedge e_j impossible. In general, no contagion is possible if

$$\Theta_\lambda > {\Theta_\lambda}^1 = 1 - \frac{1}{|e|_{\max}}, \tag{14}$$

where $|e|_{\max}$ is the largest cardinality. However, this bound tends to overestimate the true threshold. For example, in Supplementary Section S2, we show an example where $|e|_{max} = 10$, but there is no transition when $\Theta_\lambda > 0.75$.

Note that these bounds are sharp for uniform regular hypergraphs. However, in the presence of heterogeneity, the boundaries of the different subcritical behaviors may be a function of the contagion and annihilation thresholds. For example, see Supplementary Figs. 3 and 4, where heterogeneity bends the boundary of the always active region.

Data availability

The Telegram hypergraph used in this paper is available at https://zenodo.org/records/15674015.

Code availability

The code used to perform the simulations and the results in this paper are available at https://doi.org/10.5281/zenodo.18468019.

References

1. Allen, J., Howland, B., Mobius, M., Rothschild, D. & Watts, D. J. Evaluating the fake news problem at the scale of the information ecosystem. *Sci. Adv.* **6**, eaay3539 (2020).
2. Lorenz-Spreen, P., Oswald, L., Lewandowsky, S. & Hertwig, R. A systematic review of worldwide causal and correlational evidence on digital media and democracy. *Nat. Hum. Behav.* **7**, 74–101 (2023).
3. Zhang, Z.-K. et al. Dynamics of information diffusion and its applications on complex networks. *Phys. Rep.* **651**, 1–34 (2016).
4. Aïmeur, E., Amri, S. & Brassard, G. Fake news, disinformation and misinformation in social media: a review. *Soc. Netw. Anal. Min.* **13**, 30 (2023).
5. Meel, P. & Vishwakarma, D. K. Fake news, rumor, information pollution in social media and web: a contemporary survey of state-of-the-arts, challenges and opportunities. *Expert Syst. Appl.* **153**, 112986 (2020).
6. Bradshaw, S. & Howard, P. N. *The Global Disinformation Order: 2019 Global Inventory of Organised Social Media Manipulation*. Technical Report. (University of Oxford, 2019).
7. Battiston, F. et al. The physics of higher-order interactions in complex systems. *Nat. Phys.* **17**, 1093–1098 (2021).
8. Ferraz de Arruda, G., Aleta, A. & Moreno, Y. Contagion dynamics on higher-order networks. *Nat. Rev. Phys.* **6**, 468–482 (2024).
9. Neuhäuser, L., Lambiotte, R. & Schaub, M. T. Consensus dynamics on temporal hypergraphs. *Phys. Rev. E* **104**, 064305 (2021).
10. Carletti, T., Battiston, F., Cencetti, G. & Fanelli, D. Random walks on hypergraphs. *Phys. Rev. E* **101**, 022308 (2020).
11. Iacopini, I., Petri, G., Barrat, A. & Latora, V. Simplicial models of social contagion. *Nat. Commun.* **10**, 2485 (2019).
12. de Arruda, G. F., Petri, G. & Moreno, Y. Social contagion models on hypergraphs. *Phys. Rev. Res.* **2**, 023032 (2020).
13. Higham, D. J. & de Kergorlay, H.-L. Mean field analysis of hypergraph contagion models. *SIAM J. Appl. Math.* **82**, 1987–2007 (2022).
14. Ferraz de Arruda, G., Petri, G., Rodriguez, P. M. & Moreno, Y. Multistability, intermittency, and hybrid transitions in social contagion models on hypergraphs. *Nat. Commun.* **14**, 1375 (2023).
15. Kiss, I. Z., Iacopini, I., Simon, P. L. & Georgiou, N. Insights from exact social contagion dynamics on networks with higher-order structures. *J. Complex Netw.* **11**, cnad044 (2023).
16. Jhun, B. Effective epidemic containment strategy in hypergraphs. *Phys. Rev. Res.* **3**, 033282 (2021).
17. St-Onge, G. et al. Influential groups for seeding and sustaining nonlinear contagion in heterogeneous hypergraphs. *Commun. Phys.* **5**, 25 (2022).
18. Mancastroppa, M., Iacopini, I., Petri, G. & Barrat, A. Hyper-cores promote localization and efficient seeding in higher-order processes. *Nat. Commun.* **14**, 6223 (2023).
19. Kim, J.-H. & Goh, K.-I. Higher-order components dictate higher-order contagion dynamics in hypergraphs. *Phys. Rev. Lett.* **132**, 087401 (2024).
20. Centola, D., Becker, J., Brackbill, D. & Baronchelli, A. Experimental evidence for tipping points in social convention. *Science* **360**, 1116–1119 (2018).
21. Daley, D. J. & Kendall, D. G. Epidemics and rumours. *Nature* **204**, 1118–1118 (1964).
22. Maki, D. P. & Thomson, M. *Mathematical Models and Applications: With Emphasis on the Social, Life, and Management Sciences* (Prentice-Hall Inc., 1973).
23. Baumgartner, J., Zannettou, S., Squire, M. & Blackburn, J. The Pushshift Telegram dataset. In *Proc. International AAAI Conference on Web and Social Media* Vol. 14, 840–847 (Association for the Advancement of Artificial Intelligence (AAAI), 2020).
24. Notarmuzi, D., Castellano, C., Flammini, A., Mazzilli, D. & Radicchi, F. Universality, criticality and complexity of information propagation in social media. *Nat. Commun.* **13**, 1308 (2022).
25. Van Mieghem, P., Omic, J. & Kooij, R. Virus spread in networks. *IEEE/ACM Trans. Netw.* **17**, 1–14 (2009).
26. de Arruda, G. F., Rodrigues, F. A. & Moreno, Y. Fundamentals of spreading processes in single and multilayer complex networks. *Phys. Rep.* **756**, 1–59 (2018).
27. Ferraz de Arruda, G., Jeub, L. G. S., Mata, A. S., Rodrigues, F. A. & Moreno, Y. From subcritical behavior to a correlation-induced transition in rumor models. *Nat. Commun.* **13**, 3049 (2022).
28. Ferraz de Arruda, G., Tizzani, M. & Moreno, Y. Phase transitions and stability of dynamical processes on hypergraphs. *Commun. Phys.* **4**, 24 (2021).
29. Landry, N. W. & Restrepo, J. G. The effect of heterogeneity on hypergraph contagion models. *Chaos Interdiscip. J. Nonlinear Sci.* **30**, 103117 (2020).
30. Benson, A. R., Abebe, R., Schaub, M. T., Jadbabaie, A. & Kleinberg, J. Simplicial closure and higher-order link prediction. *Proc. Natl. Acad. Sci. USA.* **115**, E11221–E11230 (2018).
31. Granovetter, M. & Soong, R. Threshold models of diffusion and collective behavior. *J. Math. Sociol.* **9**, 165–179 (1983).
32. Malizia, F., Guzmán, A., Iacopini, I. & Kiss, I. Z. Disentangling the role of heterogeneity and hyperedge overlap in explosive contagion on higher-order networks. *Phys. Rev. Lett.* **135**, 207401 (2025).
33. Gillespie, D. T. Exact stochastic simulation of coupled chemical reactions. *J. Phys. Chem.* **81**, 2340–2361 (1977).
34. Kuryliak, Y., Emmerich, M. T. & Dosyn, D. Simulating epidemic peak dynamics on complex networks using efficient Gillespie algorithms. *Infect. Genet. Evol.* **132**, 105768 (2025).
35. Maia, H. P., Cota, W., Moreno, Y. & Ferreira, S. C. Efficient Gillespie algorithms for spreading phenomena in large and heterogeneous higher-order networks. Preprint at *arXiv* https://doi.org/10.48550/arXiv.2509.20174 (2025).
36. Oliveira, K. A., Traversa, P., Ferraz de Arruda, G. & Moreno, Y. Software code for the rumor propagation model on hypergraphs. https://doi.org/10.5281/zenodo.18468019 (2026).
37. Chodrow, P. S. Configuration models of random hypergraphs. *J. Complex Netw.* **8**, cnaa018 (2020).
38. Traversa, P., de Arruda, G. F. & Moreno, Y. From unbiased to maximal-entropy random walks on hypergraphs. *Phys. Rev. E* **109**, 054309 (2024).

Acknowledgements

K.A.O. was partially supported by the European Union through an ERC grant (ID-COMPRESSION, grant number: 101124175). Views and opinions expressed are, however, those of the author(s) only and do not necessarily reflect those of the European Union or the European Research Council Executive Agency. Neither the European Union nor the granting authority can be held responsible for them. G.F.A. was supported by the São Paulo Research Foundation (FAPESP), Process Numbers 2024/16711-8 and 2025/04409-8. P.T. and Y.M. were partially supported by the Government of Aragón, Spain, and "ERDF A way of making Europe" through grant E36-23R (FENOL), and by Ministerio de Ciencia, Innovación y Universidades, Agencia Española de Investigación (MICIU/AEI/10.13039/501100011033) Grant No. PID2023-149409NB-I00. The authors acknowledge the use of the computational resources of COSNET Lab at Institute BIFI, which were funded by Banco Santander (grant Santander-UZ 2020/0274) and the Government of Aragón (grant UZ-164255). The funders had no role in study design, data collection and analysis, decision to publish, or preparation of the manuscript.

Author contributions

Conceptualization: K.A.O., P.T., G.F.A., and Y.M.; methodology: K.A.O., P.T., G.F.A., and Y.M.; investigation: K.A.O., P.T., G.F.A., and Y.M.; writing—original draft: K.A.O., P.T., G.F.A., and Y.M.; writing—review and editing: K.A.O., P.T., G.F.A., and Y.M.; validation, formal analysis: K.A.O., P.T.,

G.F.A., and Y.M.; software: K.A.O., P.T., and G.F.A. All authors have read, edited, and approved the final manuscript

Competing interests
The authors declare no competing interests.

Additional information
Supplementary information The online version contains supplementary material available at https://doi.org/10.1038/s41467-026-70096-w.

Correspondence and requests for materials should be addressed to Yamir Moreno.

Peer review information *Nature Communications* thanks the anonymous reviewers for their contribution to the peer review of this work. A peer review file is available.

Reprints and permissions information is available at http://www.nature.com/reprints

Publisher's note Springer Nature remains neutral with regard to jurisdictional claims in published maps and institutional affiliations.

Open Access This article is licensed under a Creative Commons Attribution-NonCommercial-NoDerivatives 4.0 International License, which permits any non-commercial use, sharing, distribution and reproduction in any medium or format, as long as you give appropriate credit to the original author(s) and the source, provide a link to the Creative Commons licence, and indicate if you modified the licensed material. You do not have permission under this licence to share adapted material derived from this article or parts of it. The images or other third party material in this article are included in the article's Creative Commons licence, unless indicated otherwise in a credit line to the material. If material is not included in the article's Creative Commons licence and your intended use is not permitted by statutory regulation or exceeds the permitted use, you will need to obtain permission directly from the copyright holder. To view a copy of this licence, visit http://creativecommons.org/licenses/by-nc-nd/4.0/.

© The Author(s) 2026